

# Charge ordering in quarter-filled ladder systems coupled to the lattice

M. Aichhorn,<sup>1</sup> M. Hohenadler,<sup>1</sup> E. Ya. Sherman,<sup>1,2</sup> J. Spitaler,<sup>2</sup> C. Ambrosch-Draxl,<sup>2</sup> and H. G. Evertz<sup>1</sup>

<sup>1</sup>*Institut für Theoretische Physik, Technische Universität Graz, Petersgasse 16, A-8010 Graz, Austria*

<sup>2</sup>*Institut für Theoretische Physik, Karl-Franzens-Universität Graz, Universitätsplatz 5, A-8010 Graz, Austria*

We investigate charge ordering in the presence of electron-phonon coupling for quarter-filled ladder systems by using exact diagonalization. As an example we consider  $\text{NaV}_2\text{O}_5$  using model parameters obtained from first-principles band-structure calculations. The relevant Holstein coupling to the lattice considerably reduces the critical value of the nearest-neighbor Coulomb repulsion at which formation of the zig-zag charge-ordered state occurs, which is then accompanied by a static lattice distortion. Energy and length of a kink-like excitation on the background of the distorted lattice are calculated. Spin and charge spectra on ladders with and without static distortion are obtained, and the charge gap and the effective spin-spin exchange parameter  $J$  are extracted.  $J$  agrees well with experimental results. Analysis of the dynamical Holstein model, restricted to a small number of phonons, shows that low frequency lattice vibrations have a strong influence on the charge ordering, particularly in the vicinity of the phase transition point. By investigating the charge order parameter we conclude that phonons produce dynamical zig-zag lattice distortions. A model with only static distortions gives a good description of the system well away from the transition point while overestimating the amount of charge ordering in the vicinity of the phase transition.

PACS numbers: 71.10.Fd, 71.38.-k, 63.22.+m

## I. INTRODUCTION

The formation of an ordered pattern of ion charges is a rather general type of phase transition which occurs in three- as well as lower-dimensional solids. It has been known for more than six decades<sup>1</sup> since its discovery in magnetite  $\text{Fe}_3\text{O}_4$ . Even in that compound this phenomenon still attracts a lot of attention due to the interesting physics of the transition. Since the charge ordering causes changes in the interaction between the ions, it drives a lattice distortion, which, in turn, influences the ordering pattern. The quarter-filled ladder compound  $\text{NaV}_2\text{O}_5$  (Ref. 2) is another interesting example of a system which shows charge ordering. Here the transition, as observed in the nuclear magnetic resonance experiments,<sup>3</sup> occurs at  $T_{\text{CO}} \approx 35$  K and is accompanied by the formation of a spin gap<sup>4</sup> at the same<sup>5</sup> or slightly lower temperature. In  $\text{NaV}_2\text{O}_5$ , where one  $d_{xy}$  electron is shared by two V ions in a V-O-V rung, the ordering occurs as a static charge disproportion  $\delta$  between the V ions, which obtain charges  $4.5 \pm \delta$  with a zig-zag pattern of  $\delta$ 's. Most probably, the main driving force for the transition is the Coulomb repulsion of electrons on the nearest-neighbor sites within one leg of the ladder. For half the ladders the apical oxygen ion is located below the ladder and for the other half above. Therefore the crystal environment of the V ions is asymmetric, and the  $d_{xy}$  electron is subject to a strong Holstein-like electron-phonon coupling.<sup>6</sup> As a result, the transition is accompanied by the displacement of ions from their positions in the high-temperature phase ( $T > T_{\text{CO}}$ ). They then form a larger unit cell, as clearly seen directly in the x-ray diffraction experiments,<sup>7</sup> where displacements of V ions of the order of  $0.05 \text{ \AA}$  were observed, and indirectly in the appearance of new phonon modes in the infrared

absorption<sup>8</sup> and Raman scattering spectra.<sup>9</sup>

The importance of the coupling to the lattice for phase transitions in quarter-filled systems was shown in Refs. 10,11. The low-energy excitations of the zig-zag order parameter are also strongly influenced by the lattice.<sup>12</sup>

The static properties of the ground state of the doped ladders without coupling to lattice distortions were extensively investigated using mean field approaches,<sup>13,14,15</sup> the density-matrix renormalization-group (DMRG),<sup>16</sup> bosonization, and renormalization group techniques.<sup>17</sup> The DMRG studies show that at strong enough Hubbard interaction the ladders exhibit a zig-zag charge order if the repulsion between the electrons on the nearest-neighbor sites exceeds some critical value  $V_c$ . The corresponding phase transition is of second-order as a function of  $V$ . For a very strong intersite repulsion, phase separation becomes possible.<sup>16</sup> Dynamical properties were studied with exact numerical diagonalization<sup>18,19,20</sup> without taking into account the coupling to the lattice. They were quite successful in understanding  $\text{NaV}_2\text{O}_5$  dynamical properties above the transition temperature.

The investigation of the ordering of electrons interacting with the lattice requires the knowledge of electron-phonon couplings and lattice force constants in addition to electronic parameters such as hopping matrix elements and electron correlations. For a given compound almost all of these parameters can be extracted from first-principles band-structure calculations. The force constants and electron-phonon coupling can be obtained by comparing the total energies and the interionic forces in distorted and undistorted lattices. The phonon frequencies required for studies of dynamical lattice distortions are given by experiment,<sup>9</sup> while the necessary knowledge of their eigenvectors can be obtained from first-principles

calculations. We performed such calculations of the band structure, lattice dynamics and electron-phonon coupling for the  $\text{NaV}_2\text{O}_5$  compound. These calculations are in good agreement with Ref. 2 in the part concerning the band structure, and their details as well as a comparison to other first-principles calculations<sup>21</sup> will be published elsewhere.<sup>22</sup> In the present paper we will concentrate on the strongest electron-phonon mode present in  $\text{NaV}_2\text{O}_5$ , which is a simple Holstein-type interaction.<sup>22</sup>

We therefore investigate a model which takes into account the main interactions, i.e., the Hubbard and intersite repulsions and the coupling to the lattice. We study the ground-state properties of a quarter-filled ladder coupled to static lattice distortion with the Lanczos algorithm. We show that the ordering is strongly enhanced by the interaction with the lattice for realistic values of the coupling. Secondly, the interaction with dynamical (quantum) phonons at different frequencies within the Holstein model is considered. We find that indeed, the quantum phonons produce and stabilize the static order.

The paper is organized as follows. In Sec. II we introduce the extended Hubbard model (EHM) with additional lattice distortions. In Sec. III we present results for static properties of this model, including kink excitations. Dynamical quantities are discussed in Sec. IV. Section V focuses on the influence of dynamical phonons, and finally we give our conclusions in Sec. VI.

## II. MODEL

The quarter-filled ladder compound  $\alpha'$ - $\text{NaV}_2\text{O}_5$  can be described microscopically by an extended Hubbard (or  $t$ - $U$ - $V$ ) model (EHM). For the description of the distorted low-temperature phase we also include the coupling of electrons to the lattice, yielding the model

$$H = H_{\text{EHM}} + H_l + H_{e-l}, \quad (1)$$

where  $H_l$  is the lattice deformation contribution, and  $H_{e-l}$  the electron-lattice interaction. These terms are given by

$$H_{\text{EHM}} = - \sum_{\langle ij \rangle, \sigma} t_{ij} (c_{i\sigma}^\dagger c_{j\sigma} + \text{H.c.}) + U \sum_i n_{i\uparrow} n_{i\downarrow} + \sum_{\langle ij \rangle} V_{ij} n_i n_j, \quad (2a)$$

$$H_l = \kappa \sum_i \frac{z_i^2}{2}, \quad (2b)$$

$$H_{e-l} = -C \sum_i z_i n_i, \quad (2c)$$

with the effective lattice force constant  $\kappa$  and the Holstein constant  $C$ . The sites are labeled by the indices  $i, j$  and  $z_i$  is the distortion on site  $i$ . The hopping matrix elements  $t_{ij}$  connect nearest neighbor sites  $\langle ij \rangle$  (see Fig. 1) with occupation numbers  $n_i = n_{i\uparrow} + n_{i\downarrow}$ .

The first-principles calculations done in Ref. 2 and by our group<sup>22</sup> yield the intrarung hopping  $t_a \approx 0.35$  eV, which we will use below as the unit of energy. For the hopping along the ladder we use  $t_b = t_a/2$ , again in agreement with the band-structure results,<sup>2,22</sup> whereas previous DMRG studies<sup>16</sup> were mostly done at  $t_a/t_b \leq 1.4$ . For the on-site Coulomb interaction we use  $U = 8.0$  as estimated in Ref. 2. We assume  $V_{ij} = V$  to be the same for all bonds, and take  $V$  as a free parameter since there is no unique procedure of extracting it from the band-structure calculations. The lattice distortions are expressed in units of  $0.05 \text{ \AA}$  since the ion displacement below  $T_{\text{CO}}$  are of this order of magnitude.<sup>7</sup> With the chosen units of energy and length the comparison of the band structure and lattice force calculations done on distorted and undistorted lattices give the dimensionless constants  $\kappa = 0.125$  and  $C = 0.35$ , respectively.<sup>22</sup> The effective coupling parameter  $C^2/\kappa$  is close to unity and, therefore, the lattice plays an important role in determining the properties of  $\text{NaV}_2\text{O}_5$ .

The Hamiltonian in Eq. (1) will be used for calculations with both static and dynamical lattice distortions. All quantities presented in this paper are calculated by the ground state Lanczos method on single ladders of up to eight rungs, which enabled us to perform simple finite size scaling. The largest Hilbert space for the eight rung lattice considered in this study was of dimension  $N_{\text{states}} = 1656592$ , which could be reduced in special cases by exploiting translational invariance and  $S_z$  conservation to  $N_{\text{states}} = 103820$ . The next lattice size admitting charge order would consist of ten rungs, which is far beyond our computational capabilities. The restriction to a single ladder is a considerable simplification compared to the structure of  $\text{NaV}_2\text{O}_5$ , but for the quantities of interest in this paper the role of other ladders is of minor importance, since the frustration of the ladder-ladder interactions significantly reduces their effect in the zig-zag ordered state.

## III. STATIC PROPERTIES

### A. Charge order

To investigate the connection between the lattice distortion and charge ordering we calculated the static charge structure factor

$$S_c(\mathbf{q}) = \frac{1}{N} \sum_{ij} e^{i\mathbf{q}(\mathbf{R}_i - \mathbf{R}_j)} (\langle n_i n_j \rangle - \langle n \rangle^2), \quad (3)$$

where  $N$  is the total number of sites in the system. The zigzag charge order parameter  $m_{\text{CO}}$  can be expressed in terms of this structure factor as

$$m_{\text{CO}}^2 = \frac{1}{N \langle n \rangle^2} S_c(\mathbf{Q}), \quad \mathbf{Q} = (\pi, \pi). \quad (4)$$

The term  $\langle n \rangle^2$  in the denominator ensures that the order parameter is equal to unity for full ordering, which in

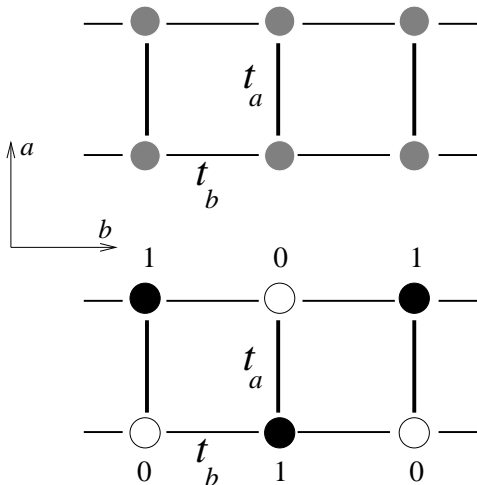


FIG. 1: Schematic picture of ladders, with hopping matrix elements  $t_a$  on the rungs and  $t_b$  along the chains. The darkness of the circles corresponds to the charges on the sites of the ladder. The upper ladder is shown without charge order, the lower ladder with zigzag charge order.

$\text{NaV}_2\text{O}_5$  corresponds to the charges of V ions within a rung to be equal to +5 and +4, respectively.

At this point the lattice distortions  $z_i$  in the Hamiltonian are external parameters of the model and not dynamical variables. Therefore they have to be fixed in a proper way, for which we chose a mean field approach. Considering the distortions as the mean field parameters one can extract the optimal value for the  $z_i$  by looking for the minimum in the ground-state energy with respect to  $z_i$ . This procedure could be done within the unrestricted Hartree-Fock approximation, but this complicates the calculation because of the larger number of variables for which the minimum has to be found. Instead we restrict ourselves to a single order pattern, the zig-zag order,<sup>13,15</sup> which was observed experimentally:<sup>7</sup>

$$z_i = ze^{i\mathbf{Q}\cdot\mathbf{R}_i}. \quad (5)$$

and investigate the total energy as a function of  $z$ . The optimal values of  $z$  where the total energy reaches the minimum for several values of the nearest-neighbor Coulomb interaction  $V$  determined in this way are indicated by arrows in Fig. 2. In the following we denote the position of the minimum in the ground-state energy by  $z_{\min}$ .

For interaction strengths of  $V = 1.5$  up to  $V = 3.0$  a clear minimum occurs at  $z \approx 1$ . Additionally one finds a maximum at  $z = 0$ , which results from the  $z \rightarrow -z$  symmetry of the system. We also found a small distortion for  $V = 1.0$ , but it is strongly size dependent and rapidly decreases with increasing length of the ladder, whereas the distortions marked by arrows in Fig. 2 are almost independent of the system size. Therefore we argue that the finite value of  $z$  at  $V = 1.0$  is due to finite-size effects and disappears in the thermodynamic limit. For this reason we did not mark it with an arrow in Fig. 2.

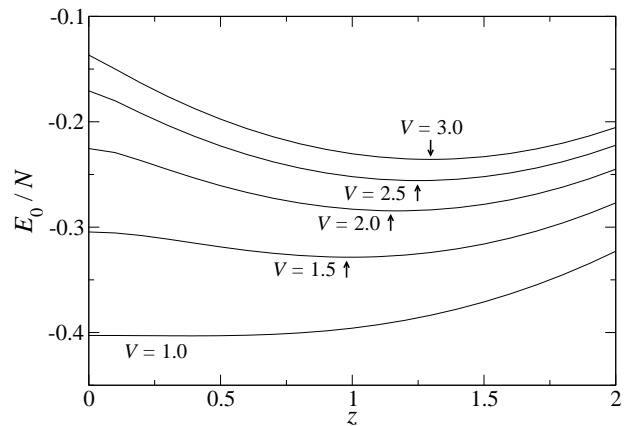


FIG. 2: Ground-state energy per site as a function of the distortion  $z$  calculated on an  $8 \times 2$  system with periodic boundary conditions along the ladder, and  $C = 0.35$ . From bottom to top:  $V = 1.0, 1.5, 2.0, 2.5, 3.0$ . The arrows indicate the position of the minimum.

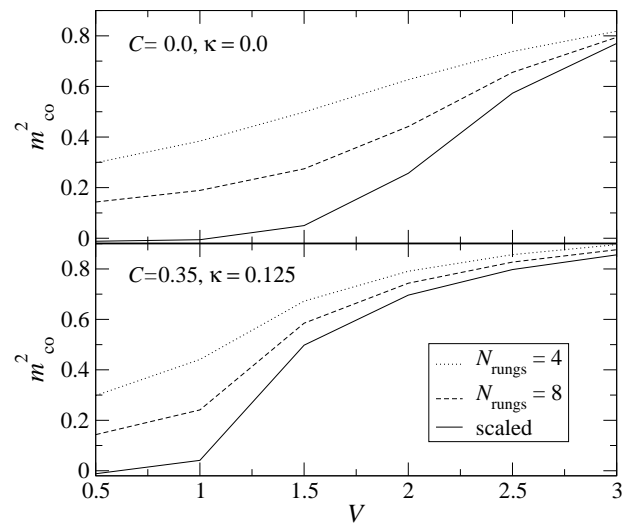


FIG. 3: Charge order parameter for several values of  $V$ . Upper/lower panel: Calculation without/with coupling to the lattice. The solid lines are obtained by  $1/N_{\text{rungs}}$  finite size extrapolation.

This behavior gives a first idea about the charge ordering of the system with and without coupling to the lattice. From Fig. 2 one could expect that the charge ordering transition in the presence of static mean-field-like lattice distortions occurs in the region between  $V = 1.0$  and  $V = 1.5$ . In order to investigate this transition we calculate the order parameter given by Eq. (4). This quantity shows strong finite-size effects, which makes it necessary to apply finite-size scaling. We calculated the order parameter for systems of four and eight rungs, respectively, the largest system size available. Although higher-order corrections to the scaling behavior are expected for these small systems, we performed a  $1/N_{\text{rungs}}$  extrapolation to  $1/N_{\text{rungs}} = 0$ . This procedure does not

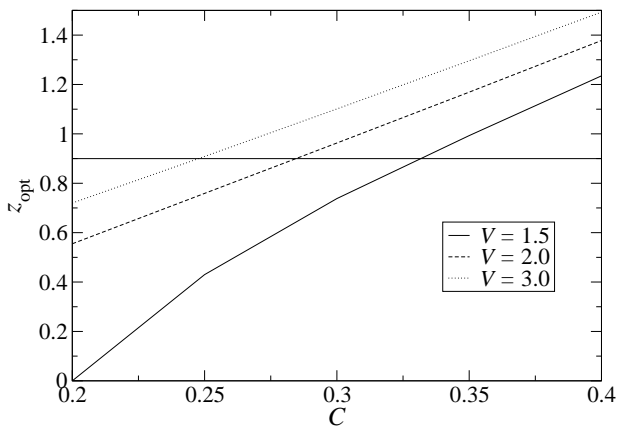


FIG. 4: Optimal distortion  $z_{\text{opt}}$  as a function of the Holstein constant  $C$  for different values of the coulomb interaction  $V$ , calculated on a  $8 \times 2$  cluster. The horizontal line indicates the experimental result.

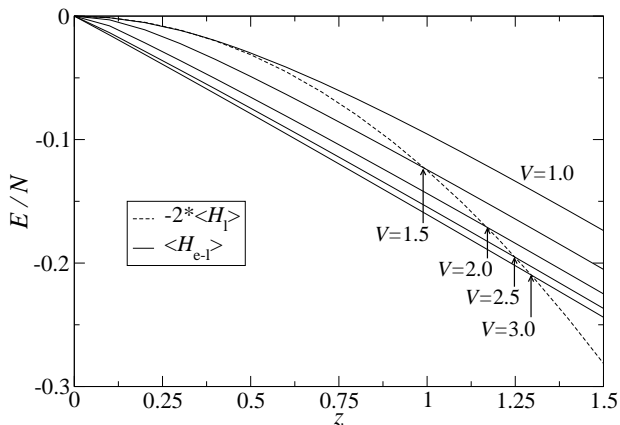


FIG. 5: Contribution of the lattice energy Eq. (2b) (dashed) and the electron-lattice energy Eq. (2c) (solid) to the ground state energy as a function of the distortion  $z$ , at  $C = 0.35$ . The lattice energy is independent of  $V$ . Electron-lattice energy, from top to bottom:  $V = 1.0, 1.5, 2.0, 2.5, 3.0$ . The arrows are drawn where the total energy has its minimum, as in Fig. 2.

give the exact value of the order parameter in the thermodynamic limit and does not allow to extract an exact value for the critical Coulomb interaction  $V_c$ , but it provides the possibility to obtain a rough estimate of the interaction  $V$  at which the phase transition occurs as well as the approximate  $m_{\text{CO}}^2(V)$ -dependence.

To study the effects of the lattice distortions we also calculated the order parameter without coupling to the lattice, that is for  $C = 0$ . The results are shown in Fig. 3. As one can see in the upper panel where no lattice distortions are present, the order parameter changes rather smoothly when going from the disordered phase into the ordered one. A different behavior can be found for finite lattice distortions. Here the charge ordering sets in, at a much lower value of  $V$  than in the absence of distur-

tions. In addition the transition sharpens considerably. For both zero and finite distortions the finite size scaled order parameter is slightly negative for small interactions  $V$ , which is due to the fact that higher order corrections in the scaling have been neglected.

The optimal distortions  $z$  for different values of the Holstein constant  $C$  and repulsion  $V$  are presented in Fig. 4. In our units the distortion found experimentally in the charge-ordered phase is at approximately  $z = 0.9$ ,<sup>7</sup> indicated by a horizontal line in Fig. 4. For  $V = 1.5$ , close to the charge order phase transition, this value of  $z = 0.9$  is reached near  $C = 0.33$ . The distortion close to  $z = 0.9$  is realized also for other interactions, e.g. deep in the ordered phase at  $V = 3.0$ ,  $C = 0.24$ . Since, however,  $\text{NaV}_2\text{O}_5$  is probably close to a quantum critical point of charge ordering,<sup>20</sup> and because of the value for  $C$  obtained from the band structure calculations, we conclude that the system can best be described in the ordered phase using  $V \approx 1.3$  and  $C \approx 0.35$ .

When calculating the ground-state energy of the system, the question arises how the terms in Eq. (1) contribute to the total energy, i.e., whether some sort of virial theorem holds. In Fig. 5 the behavior of the two contributions (2b) and (2c) is shown. One can easily see that the crossing points of the curves are at the same value of  $z$  at which the ground-state energy reaches its minimum, Fig. 2. Therefore we find that a virial theorem such as that for the one-electron polaronic states,<sup>23</sup> is fulfilled in the form

$$\langle H_l \rangle = -\frac{1}{2} \langle H_{e-l} \rangle, \quad (6)$$

with a relative numerical accuracy of better than  $10^{-4}$ . For large Coulomb interactions well above the phase transition this high accuracy is likely achieved since the ion charges depend very weakly on  $z$ . Therefore, compared to  $H_{e-l}$  and  $H_l$ ,  $H_{\text{EHM}}$  is almost independent of  $z$ , namely  $[dH_{\text{EHM}}/dz(z_{\text{min}}) \approx 0.005]$ , and the dependence of  $H_{e-l}(z)$  in Fig. 5 is close to a straight line. Then the virial theorem follows from the functional form of  $H_l(z)$  and  $H_{e-l}(z)$ . For smaller values of the interaction, e.g.,  $V = 1.5$ , the dependence of the ion charges and  $H_{\text{EHM}}$  is considerably larger  $[dH_{\text{EHM}}/dz(z_{\text{min}}) \approx 0.03]$ . Yet also in this case the virial relation is satisfied. The contribution of the sum of the lattice terms  $\langle H_l + H_{e-l} \rangle$  to the total energy varies between 19% at  $V = 1.5$  and 30% at  $V = 3.0$ .

## B. Kink excitations

So far we have considered the perfect zig-zag charge order pattern described by Eq. (5). This ordering can be destroyed by local in-rung excitations where an electron hops from the site with minimal energy to that with maximal energy, as marked by black and white circles in Fig. 1. The excitation energy of this process is  $2V$ , provided the system is totally ordered, that is,  $m_{\text{CO}} = 1.0$ .

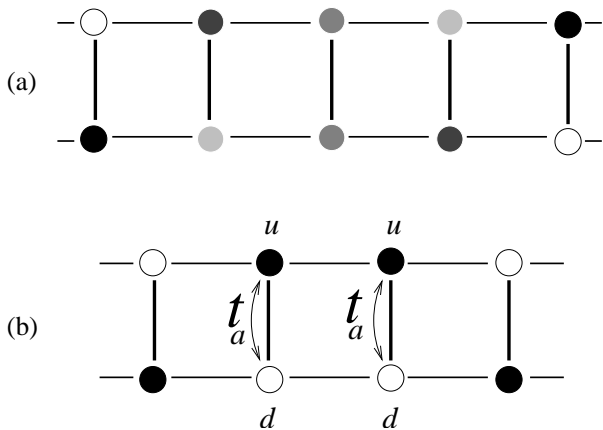


FIG. 6: (a) A schematic plot of a non-local kink-like excitation in an ordered ladder. The darkness of the circles corresponds to the charges on the sites of the ladder. (b) Local kink excitation with a sharp change of the order parameter. The electron states for one of the electrons moving between sites  $u$  and  $d$  are degenerate in this case.

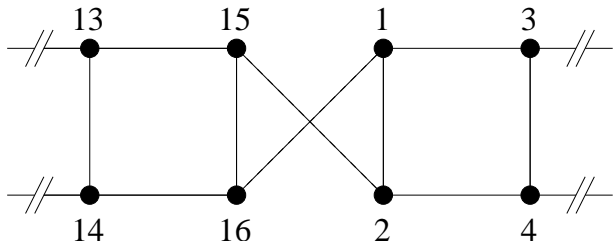


FIG. 7: Twisted ("Möbius") boundary conditions which produce a kink excitation. The numbers label the sites in the  $8 \times 2$  cluster from 1 to 16.

Another type of excitation is the formation of a local pair of doubly occupied and empty rungs, which has the same energy  $2V$  at  $m_{CO} = 1.0$ . In addition, there are nonlocal kinklike excitations, where the order parameter smoothly changes along the ladder between two degenerate patterns as shown in Fig. 6. The nonlocal character of the excitation leads to a decrease of the excitation energy. Since the lattice is coupled to ion charges by the Holstein interaction, the kinks couple to the lattice, too.

In order to investigate kink excitations we used the largest system size available, which is a single ladder consisting of eight rungs, and imposed twisted "Möbius" boundary conditions<sup>24</sup> as shown in Fig. 7. The zig-zag distortions of Eq. (5) are modified to a kink distortion

$$z_i = z e^{i\mathbf{Q} \cdot \mathbf{R}_i} \tanh \left[ \frac{(\mathbf{R}_i - \mathbf{R}_0) \hat{\mathbf{e}}_a}{L} \right], \quad (7)$$

with the center of the kink  $\mathbf{R}_0$  located in the middle between the rungs,  $L$  being its length in units of the lattice spacing, and  $\hat{\mathbf{e}}_a$  the unit vector in ladder direction. We kept  $z$  at its previous optimal value  $z_{\min}$  and varied  $L$  looking for the minimum in the ground-state energy as shown in Fig. 8.

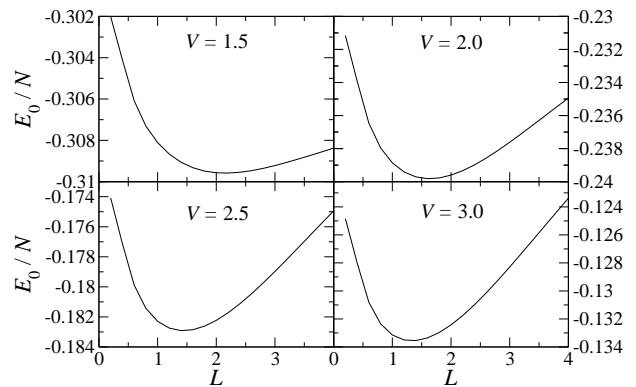


FIG. 8: Ground-state energy per site as a function of the kink length  $L$ , Eq. (7).

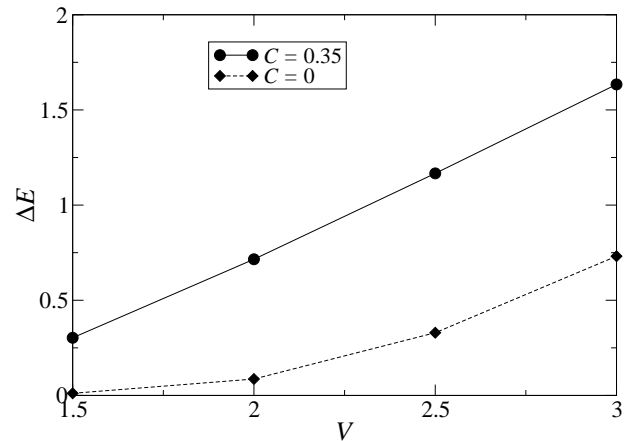


FIG. 9: Kink excitation energy as a function of the interaction  $V$ . It is zero for  $V \leq 1.0$ . The lines are guides to the eye.

For interactions up to  $V = 1.0$  the ground-state energy strongly decreases with increasing kink length  $L$ , without a minimum, implying that at this weak coupling we have no kink excitations in the system. For larger interactions we found a clear minimum in the ground-state energy. The kink length at  $V = 1.5$  is  $L \approx 2.15$ , and it shrinks to  $L \approx 1.33$  at  $V = 3.0$ .

The kink excitation energy is defined as the difference between the ground-state energy with twisted boundary conditions at the optimal value of  $L$  and the ground-state energy with periodic boundary conditions and static distortions  $z = z_{\min}$ . It is shown in Fig. 9. In the fully ordered state and in the atomic limit where  $V \gg t_a$ , the kink potential energy  $\Delta E$  is close to  $V$  (see Fig. 6). The actual total energy is considerably smaller since the kinks are extended and since at the kink boundary the electron energy on the upper ( $u$ ) and lower ( $d$ ) legs become degenerate as shown in Fig. 6, and therefore the intrarung hopping becomes more likely. The hopping kinetic energy of the order of  $-t_a$  decreases the total energy of the system, leading to the result shown in Fig. 9.

For weak interactions, where the kinks are well extended and  $m_{co}^2 \ll 1$ , our results can be compared with

a model calculation in a classical  $\phi^4$  model for infinite ladders<sup>12</sup> which gives

$$L = \frac{1}{\sqrt{V - V_c}}, \quad (8a)$$

$$\Delta E = \frac{3}{2}V(V - V_c)^{3/2}, \quad (8b)$$

where  $V_c$  is the critical value of the Coulomb interaction for the phase transition. To make a connection to our results, we estimate  $V_c$  from Eqs. (8a) and (8b) for the distorted lattice at  $V = 1.5$  and  $C = 0.35$  independently and compare them. From  $L$  and  $\Delta E$  we obtain  $V_c = 1.28$  and  $V_c = 1.05$ , respectively. These values are in reasonable agreement with each other and consistent with the behavior of the order parameter, see Fig. 3.

At all values of  $V$  the kink excitation energy with lattice coupling is larger than the excitation energy without coupling shown as dashed line in Fig. 9. This can be understood since at a fixed value of  $V > V_c$  the charge order parameter is larger for the distorted lattice. Since the ordering is more complete, the kink lengths are smaller which increases the excitation energy. Note that without lattice coupling we have no parameter  $L$  as in Eq. (7) for the determination of the kink length.

#### IV. DYNAMIC PROPERTIES

In Sec. III we only considered static properties. However, enlightening insight into the physics of the system can be extracted from dynamical correlation functions showing the spectra of charge and spin excitations. The corresponding susceptibilities are given by

$$\chi_C(\mathbf{q}, \omega) = \int dt e^{i\omega t} \langle n_{\mathbf{q}}(t) n_{-\mathbf{q}} \rangle \quad (9a)$$

$$\chi_S(\mathbf{q}, \omega) = \int dt e^{i\omega t} \langle S_{\mathbf{q}}^z(t) S_{-\mathbf{q}}^z \rangle, \quad (9b)$$

where  $n_{\mathbf{q}}(t), n_{-\mathbf{q}}$  and  $S_{\mathbf{q}}^z(t), S_{-\mathbf{q}}^z$  are the the Fourier transforms of the charge and  $z$  component of spin densities, respectively.

We calculated the charge susceptibility Eq. (9a) on a ladder consisting of eight rungs with periodic boundary conditions along the ladder. The results are shown in Fig. 10. We define the charge gap  $\Delta_C$  as the energy at which the lowest lying excitation of the charge susceptibility occurs. The corresponding momentum is always  $\mathbf{q} = \mathbf{Q}$ . In the disordered phase we have no gapless charge excitation. When increasing the Coulomb interaction  $V$ , the gap at  $\mathbf{q} = \mathbf{Q}$  decreases as shown in Fig. 11, and all other charge excitations become insignificant. The charge gap does not vanish exactly for  $C = 0$ , i.e. without coupling to the lattice, but appears to go to zero as  $N_{\text{rungs}} \rightarrow \infty$ . When the coupling to the lattice is switched on, the gap is exactly zero in the ordered phase where the symmetry is broken explicitly. The charge gap behaves in a similar way as the order

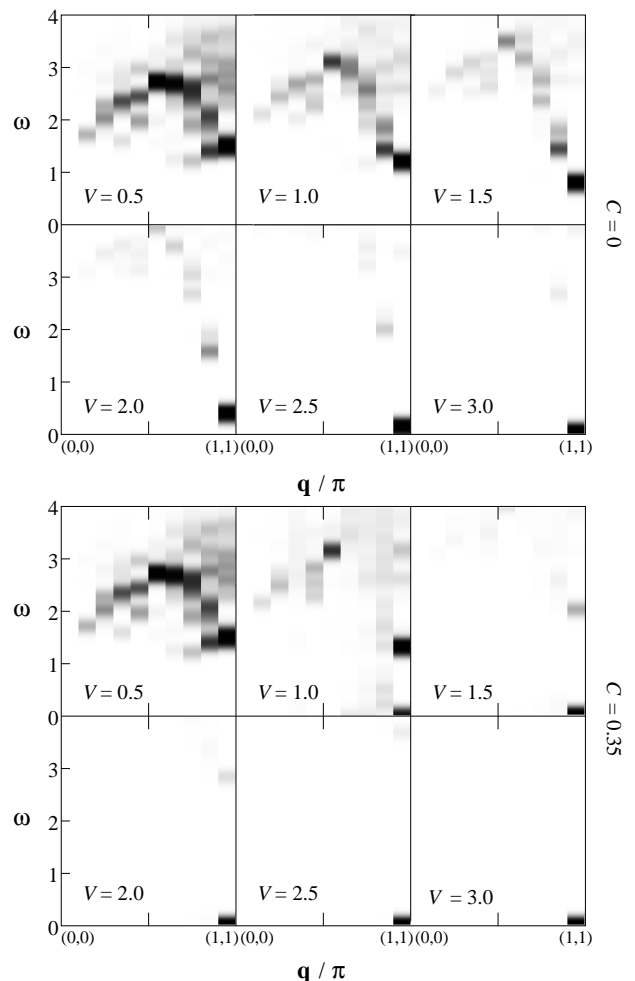


FIG. 10: Charge susceptibility calculated on an  $8 \times 2$  ladder. Upper panel: without lattice coupling. Lower panel: With lattice coupling ( $C = 0.35$ ). The wave vector scan consists of the two ranges  $(q_a, q_b)/\pi = (0, 0) \rightarrow (0, 1)$  and  $(1, 0) \rightarrow (1, 1)$ , separated by a tick mark on the horizontal axis. An additional broadening of width  $\eta = 0.1$  was used.

parameter (Fig. 3), namely, without electron-lattice coupling it changes smoothly across the phase transition, whereas the changes for finite coupling are significantly sharper.

In Fig. 10 at  $V = 1.0$ , a gapless excitation at  $\mathbf{q} = \mathbf{Q}$  can be seen, which occurs due to a small but finite distortion. As already discussed in Sec. III, this distortion is finite only due to the finite-size effects and should be zero in the thermodynamic limit.

We note that the gap  $\Delta_C$  in the charge spectrum is different from the one commonly used in DMRG calculations,  $\Delta := [E_0(N+2) - E_0(N)]/2$ , where  $E_0(N+2)$  and  $E_0(N)$  are the ground-state energies for systems consisting of  $N+2$  and  $N$  particles, respectively. Indeed, as a function of  $V$ ,  $\Delta$  shows a behavior *opposite* to  $\Delta_C$ , with  $\Delta = 0$  in the unbroken phase and  $\Delta > 0$  at large  $V$ .<sup>16</sup>

The spin susceptibility [Eq. (9b)] calculated on the same system is shown in Fig. 12. The momentum scan

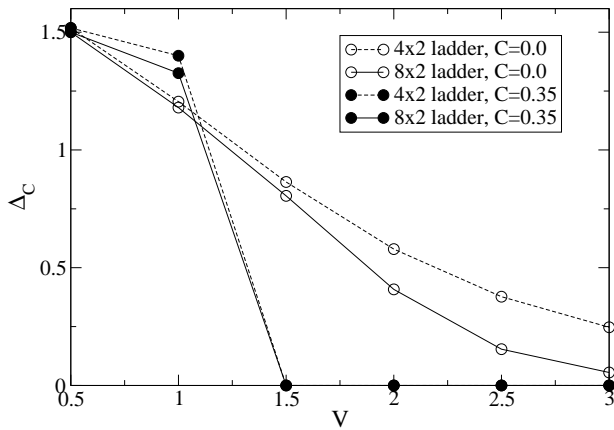


FIG. 11: Charge gap  $\Delta_C$  at  $\mathbf{q} = \mathbf{Q}$  of the charge susceptibility as a function of  $V$ . Solid lines:  $8 \times 2$  ladder. Dashed lines:  $4 \times 2$  ladder. Open symbols: Without lattice coupling. Full symbols: With lattice coupling (see text for case  $V = 1.0$ ).

consists of two ranges, from  $(q_a, q_b) = (0, 0)$  to  $(0, \pi)$ , and from  $(\pi, 0)$  to  $(\pi, \pi)$ . In the first range ( $q_a = 0$ ) one can clearly see the dispersion of an effective one-dimensional Heisenberg model, as predicted by perturbation theory.<sup>26</sup> The main change of the spin susceptibility as a function of  $V$  in this range is a decrease of the effective magnetic exchange interaction  $J_{\text{eff}}$  with increasing charge order. It can be extracted from the spin dispersion using  $J_{\text{eff}} = 2\omega(0, \pi/2)/\pi$  (Ref. 25), and is shown in Fig. 13. According to magnetic susceptibility measurements,<sup>27</sup>  $J_{\text{eff}}$  in the low-temperature phase is approximately 0.8 of the exchange in the disordered phase. Our results are in a good qualitative agreement with these data in the sense that an increase in charge order goes together with a decrease in  $J_{\text{eff}}$ .<sup>28</sup> However, a quantitative comparison cannot be made since in the experiment the ordering and, correspondingly,  $J_{\text{eff}}$ , are traced as a function of temperature for given other system parameters while we investigate the ordering at  $T = 0$  as a function of the extended Hubbard repulsion  $V$ . Our calculation also agrees well with the analytical results of Refs. 16 and 29, where it was shown that the exchange rapidly decreases with increasing  $V$ . Quantitatively, at  $V = 3, C = 0$  our results give  $J_{\text{eff}} \approx 0.06$  while perturbation theory<sup>16,29</sup> predicts  $J_{\text{eff}} \approx 0.04$ . Moreover, for  $V = 1.3, C = 0.35$ , which give a lattice distortion close to the value observed experimentally (see Fig. 4), the exchange parameter in Fig.13 is about 67 meV which is very close to the experimental 60 meV observed in the inelastic neutron scattering measurements of Ref. 31.

The second range in the spin spectrum (Fig. 12), with  $q_a = \pi$ , shows only high energy excitations at small  $V$ , but again an effective Heisenberg dispersion at large  $V$ . For small  $V$  the gap in the spin spectrum is very close to the charge gap, indicating that it is due to charge excitations. To verify this conjecture, we calculated charge and spin susceptibilities in the noninteracting limit  $V = 0$ , with  $t_b = 0$  (isolated rungs). In this case charge and spin

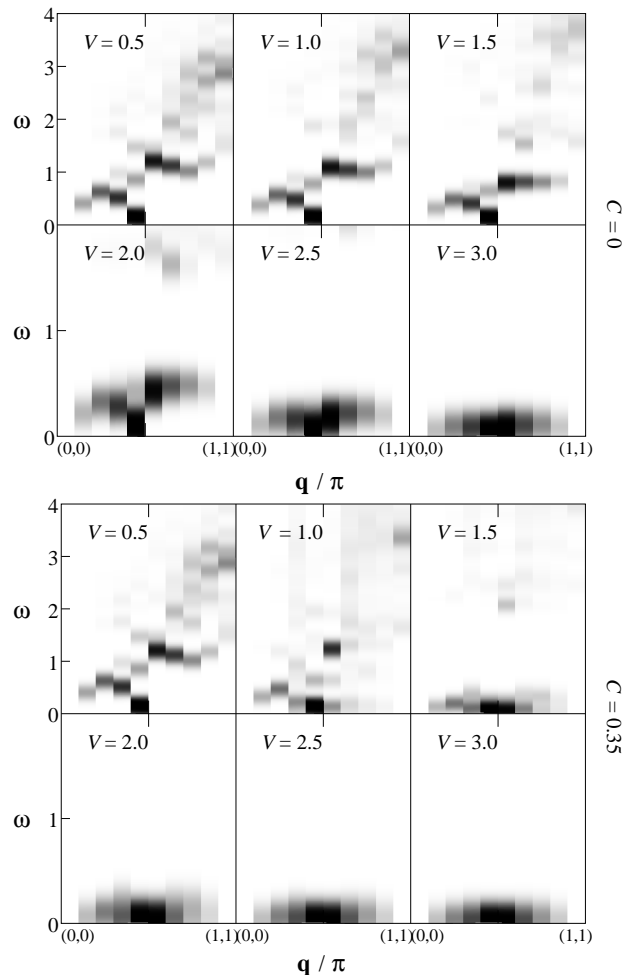


FIG. 12: Spin susceptibility calculated on an  $8 \times 2$  ladder. Upper panel: without lattice coupling. Lower panel: With lattice coupling ( $C = 0.35$ ). Presentation as in Fig. 10.

susceptibilities are equal for  $q_a = \pi$  and the gap is exactly the difference between the bonding and the antibonding state given by  $2t_a$ . Secondly, we analyzed the dependence of the spin susceptibility on the hopping  $t_b$  along the ladder in the disordered phase at  $V = 0.5$  (Fig. 14). Whereas the dispersion for  $q_a = 0$  scales as  $t_b^2$ , which is clear evidence of the magnetic origin of these excitations, the difference between the maximal and minimal excitation energy for  $q_a = \pi$  scales as  $t_b$ . These observations show a direct interplay between the spin and the dipole-active charge excitations, which is similar to the "charged" magnons introduced in Ref. 30 for interpretation of the infrared absorption spectra of  $\text{NaV}_2\text{O}_5$ .

It is interesting to note that the spin spectra in the ordered phase appear to possess a mirror symmetry with respect to the central tick mark in Fig. 12. To quantify this observation, the dispersions of the low-energy excitations at  $V = 3.0$  have been depicted in Fig. 15. The dispersions for  $q_a = 0$  and  $q_a = \pi$  are indeed very similar. Without lattice coupling the dispersion with  $q_a = \pi$  is shifted upwards compared to  $q_a = 0$  because of the small

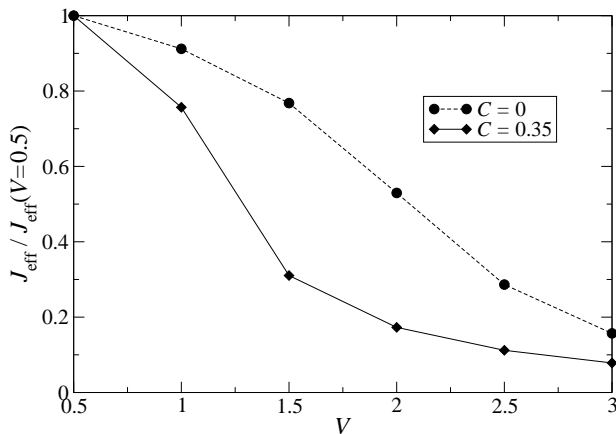


FIG. 13: Effective magnetic exchange interaction  $J_{\text{eff}}$  in ladder direction in units of  $J_{\text{eff}}(V=0.5)$  as a function of  $V$ , extracted from the spin susceptibility Eq. (9b). The interaction is shown with (solid line) and without lattice coupling (dashed line).

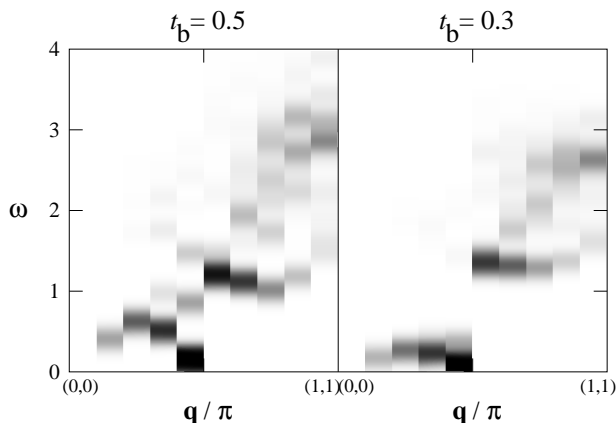


FIG. 14: Spin susceptibility in the disordered phase at  $V = 0.5$  for hopping along the ladder  $t_b = 0.5$  (left) and  $t_b = 0.3$  (right). Momentum scan as in Fig. 10.

but finite charge gap at  $V = 3.0$  (see Fig. 11). With lattice coupling and at interactions where no charge gap occurs the agreement is even better. This behavior can be understood in the following way. In the disordered phase where each electron on a rung occupies a molecular orbital consisting of two sites, momenta  $q = (0, \pi)$  and  $q = (\pi, 0)$  are not equivalent (same spin on the two sites of the rung, versus opposite spin on two sites of neighboring rungs). In this phase pure spin excitations with  $q_a = \pi$  are not possible since they require different spins on different sites within a rung. This could be achieved only by exciting another electronic state within the rung, which has the energy  $2t_a$ . In the totally zig-zag ordered state where the electrons are located on one site of the rung, these momenta become equivalent. The same holds for momenta  $q = (0, 0)$  and  $q = (\pi, \pi)$ .

The overall effect of charge ordering on the dynamical susceptibilities can best be seen by comparing the plots

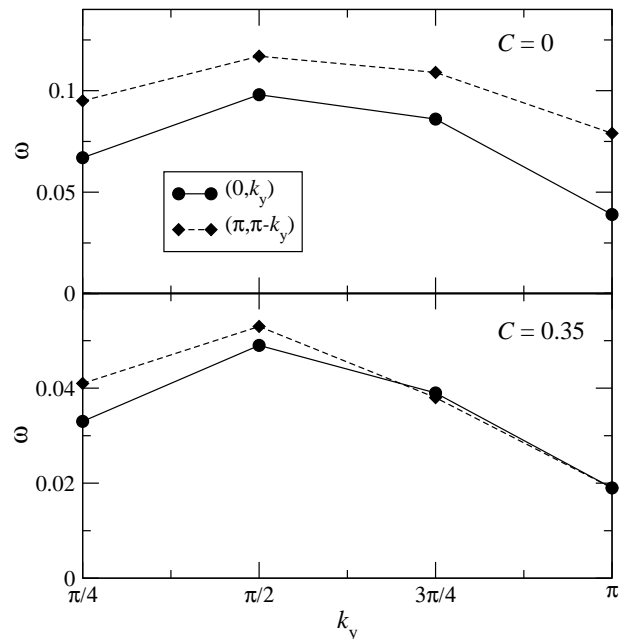


FIG. 15: Spin dispersion in the ordered phase at  $V = 3.0$  extracted from Fig. 12. Bottom: with lattice coupling, top: without lattice coupling. Direction of momentum scans: Solid lines:  $(0, 0) \rightarrow (0, \pi)$ , dashed lines:  $(\pi, \pi) \rightarrow (\pi, 0)$ .

for  $V = 2.5, C = 0.0$  and  $V = 1.5, C = 0.35$ , where the values of the order parameter are similar, see Fig. 3. The spin and charge excitations shown in these plots are qualitatively the same and the susceptibilities differ only slightly on a few points. From these figures we conclude that the dynamical spin and charge susceptibilities of the system mainly depend on the order parameter but not on the way in which the order has been achieved.

## V. HUBBARD-HOLSTEIN MODEL

So far we have only considered static distortions of the lattice. Although this is a good approximation if the dynamic fluctuations around these equilibrium positions are small, quantum phonon effects can play an important role, especially in the critical region. In this section, we therefore consider the extended Hubbard-Holstein model (EHHM)

$$H = H_{\text{EHM}} + \sum_i \left[ \frac{1}{2M} \hat{p}_i^2 + \frac{\kappa}{2} \hat{z}_i^2 - C \hat{z}_i n_i \right], \quad (10)$$

with  $H_{\text{EHM}}$  defined in Eq. (2a) and  $M$  being the mass of the local oscillators. The operators  $\hat{z}_i$  and  $\hat{p}_i$  are the coordinate and momentum of the ion on lattice site  $i$ , and all other quantities are defined in Eq. (1). When expressed in phonon creation and annihilation operators, it reads (up to a constant)

$$H = H_{\text{EHM}} + \omega_0 \sum_i b_i^\dagger b_i - g \sum_i (b_i^\dagger + b_i) n_i. \quad (11)$$



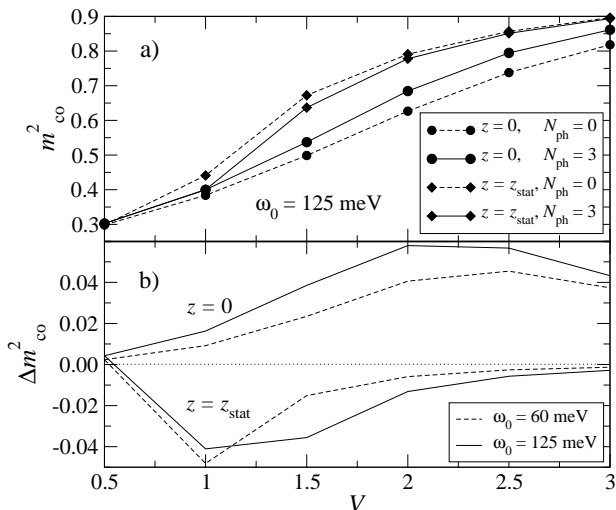


FIG. 16: (a) Order parameter  $m_{CO}^2$ , calculated on a cluster with four rungs. Phonon parameters are  $C = 0.35$ ,  $\kappa = 0.125$ , and  $\omega_0 = 125$  meV. Parameters are chosen as shown in the caption. (b)  $\Delta m_{CO}^2 = m_{CO}^2(N_{ph} = 3) - m_{CO}^2(N_{ph} = 0)$  for two phonon frequencies  $\omega_0 = 60$  and 125 meV. Upper two curves: Without static distortion. Lower two curves: with static distortion. The dotted line marks  $\Delta m_{CO}^2 = 0$ .

Here  $b_i^\dagger$  ( $b_i$ ) creates (annihilates) a phonon of frequency  $\omega_0$  (with  $\hbar = 1$ ) at lattice site  $i$ , and the phonons are locally coupled to the electron density with coupling strength  $g = C\sqrt{\omega_0/2\kappa}$ .

We would like to point out that the nature of the local phonon mode in Eq. (11) is not specified and could correspond to one of several phonon modes in the vanadates. Clearly, the use of dispersionless Einstein phonons neglects any coupling between lattice distortions of neighboring sites. However, a coupling of the Holstein type is the strongest phonon mode in  $\text{NaV}_2\text{O}_5$ .<sup>22</sup> It also represents the simplest model for electron-phonon interactions, and has been successfully used to describe the physics of other transition metal oxides such as the manganites.<sup>32</sup>

Compared to exact diagonalization of the model described by the Hamiltonian in Eq. (1), an additional difficulty arises in the case of the EHHM since the number of phonons is not conserved. Consequently, even for a finite number of lattice sites, the Hilbert space contains an infinite number of states, and has to be truncated in some way in order to apply the Lanczos method. For this reason the size of the systems which can be investigated is also considerably reduced. We restricted ourselves to a lattice with four rungs and chose a subset of the phonon states as<sup>33,34</sup>

$$|r\rangle_{\text{ph}} = \prod_{i=1}^N \frac{1}{\sqrt{\nu_i^{(r)}!}} \left(b_i^\dagger\right)^{\nu_i^{(r)}} |0\rangle_{\text{ph}}, \quad (12)$$

where  $\nu_i^{(r)}$  denotes the number of phonons at lattice site  $i$  and  $|0\rangle_{\text{ph}}$  is the phonon vacuum state. Alternatively,

the basis states could also be formulated in momentum space as in Ref. 33.

Now the truncation of the Hilbert space consists of restricting the total number of phonons in the  $|r\rangle_{\text{ph}}$  subset as

$$\sum_{i=1}^N \nu_i^{(r)} \leq N_{\text{ph}} \quad (13)$$

leading to  $(N_{\text{ph}} + N - 1)!/[N_{\text{ph}}!(N - 1)!]$  allowed phonon configurations for  $N$  sites. We would like to point out that the set of basis states in Eqs. (12) and (13) consists of all possible phonon states with up to  $N_{\text{ph}}$  phonons excited. In particular, the Hilbert space includes all linear combinations of such states.

Usually,  $N_{\text{ph}}$  is increased until convergence of an observable of interest  $O$  is achieved. The latter can be monitored by calculating the relative error  $|O(N_{\text{ph}} + 1) - O(N_{\text{ph}})|/|O(N_{\text{ph}})|$ .

Due to the complexity of the EHHM and the value of parameters, it is not possible to include enough phonon states to obtain converged results. Nevertheless, as in the case of the pure Holstein model<sup>35</sup> it is still possible to deduce the tendency of the results as  $N_{\text{ph}}$  is increased and thereby obtain information about the exact results (corresponding to  $N_{\text{ph}} = \infty$ ).

To reduce the required number of dynamical phonons, it is expedient to introduce static distortions  $z_i$  as a coordinate transformation  $\hat{z}_i = z_i + \hat{x}_i$  so that quantum fluctuations  $\hat{x}_i$  take place around the position  $z_i$ . Applying this transformation to Eq. (10) yields

$$H = H_{\text{EHHM}} + \sum_i \left[ \frac{\kappa}{2} z_i^2 - C z_i n_i \right] + \sum_i \left[ \frac{1}{2M} \hat{p}_i^2 + \frac{\kappa}{2} \hat{x}_i^2 + (\kappa z_i - C n_i) \hat{x}_i \right], \quad (14)$$

which in second quantization results in an expression analogous to Eq. (11). Note that the first line in the above equation is the same as Eq. (1). For the static distortions  $z_i$  we again use the zig-zag order pattern (5) and determine the optimal value of  $z$  by minimizing the ground-state energy in the presence of phonons yielding a static distortion  $z_{\text{stat}}$ , which is related to  $z_{\text{min}}$  introduced in Sec. III by  $z_{\text{min}} = z_{\text{stat}}(N_{\text{ph}} = 0)$ .

Note that we perform this coordinate transformation only because the number of phonons accessible in our calculations is very small, and in this case it is better to start from a different equilibrium position  $z = z_{\text{stat}}$  and not from  $z = 0$ . If it were possible to use  $N_{\text{ph}} = \infty$ , this coordinate transformation would have no influence on the physical results and the actual lattice distortions would be produced by the dynamical phonons as a coherent state of oscillators associated with the ions, independent of any initial coordinate transformation. Of course the broken symmetry would only occur in the thermodynamic limit, while correlations of the phonon positions exist already on finite lattices.

The effect of dynamical phonons on the charge order parameter is shown in Fig. 16. We did calculations for several values of  $V$  at phonon frequencies  $\omega_0 = 60$  meV and  $\omega_0 = 125$  meV, the two most relevant modes in  $\text{NaV}_2\text{O}_5$ .<sup>22</sup> The smaller frequency belongs to a collective vibration which includes displacements of the vanadium and oxygen ions, whereas the larger one corresponds to a vibration of the apical oxygen along the  $z$  axis.

From the upper panel of Fig. 16 one can easily see that for the nontransformed coordinates (circles) the inclusion of dynamical phonons with  $\omega_0 = 125$  meV considerably increases the charge ordering. Calculations with  $N_{\text{ph}} = 1$  and 2 (not shown) revealed that the increase is monotonic in the number of phonon states and we conclude that for convergence many more phonon states would be necessary. For the distorted lattice (diamonds), the dynamical phonons actually decrease the charge ordering for  $V \geq 1.0$ , and the strongest effect occurs in the vicinity of the phase transition at  $V = 1.0$  and  $V = 1.5$ . The reason for this decrease is that  $z_{\text{stat}}$  is shifted downwards with increasing number of dynamical phonons. At  $V = 1.0$ , where a finite  $z_{\text{stat}}$  at  $N_{\text{ph}} = 0$  is a finite size effect (Sec. III A),  $z_{\text{stat}}$  is reduced to zero for  $N_{\text{ph}} = 3$ . At  $V \geq 1.5$  the relative change in  $z_{\text{stat}}$  is similar to that in  $m_{\text{CO}}^2$  (Fig. 16). We want to mention that the two solid curves in the upper panel of Fig. 16 give an upper and a lower boundary for the actual value of the order parameter on the four rung lattice, since for  $N_{\text{ph}} \rightarrow \infty$  results for  $z = 0$  and  $z = z_{\text{stat}}$  become equivalent, as discussed above.

In the lower panel of Fig. 16 the difference  $\Delta m_{\text{CO}}^2$  of the order parameter in the presence of dynamical phonons to  $N_{\text{ph}} = 0$  is shown including data for  $\omega_0 = 60$  meV. For  $z = 0$  (upper two curves) this deviation is positive and the effect is always larger for  $\omega_0 = 125$  meV, which corresponds to a larger value of  $g$ . For  $z = z_{\text{stat}}$  (lower two curves) it is negative for  $V \geq 1.0$ . The crossing at  $V = 1.0$  is due to the small finite value of  $z_{\text{stat}}$  for  $N_{\text{ph}} = 0$ , i.e., a finite size effect.

It is interesting to study the order pattern of the dynamically induced distortions. For this purpose we define the correlation function

$$C_z = \frac{1}{N^2} \sum_{ij} e^{i\mathbf{Q}(\mathbf{R}_i - \mathbf{R}_j)} \left\langle (\hat{z}_i - \langle \hat{z}_i \rangle) (\hat{z}_j - \langle \hat{z}_j \rangle) \right\rangle, \quad (15)$$

which measures the zig-zag ordering of the lattice distortions, similar to Eq. (4) for the charge densities. For the nontransformed coordinates it is depicted in Fig. 17 for  $\omega_0 = 125$  meV and different numbers of dynamical phonons. From this figure it is clear that dynamical phonons induce zig-zag lattice distortions which strongly increase around the phase transition point. Note that the correlation function  $C_z$  is not normalized to the interval  $[0, 1]$  since lattice distortions are not conserved quantities, different from, e.g., charges.

For the transformed coordinates we can calculate the dynamically induced zig-zag distortions  $z_{\text{dyn}}$  directly from the expectation values  $\langle \hat{z}_i \rangle$  since the symmetry of

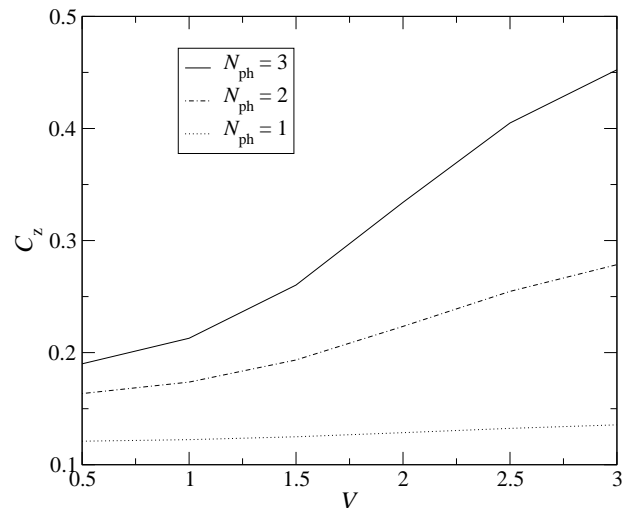


FIG. 17: Correlation function  $C_z$  as defined in Eq. (15) without static distortions for  $\omega_0 = 125$  meV. The number of phonons is given in the caption.

the system is broken explicitly. Results show that the sum  $z_{\text{tot}} = z_{\text{stat}} + z_{\text{dyn}}$  of the static distortion and the dynamically induced distortion is always smaller than the value  $z_{\text{min}}$  determined in Sec. III A, and this effect is most pronounced near the phase transition. For  $V = 1.5$  and  $N_{\text{ph}} = 3$  we got  $z_{\text{stat}} = 0.889$  and  $z_{\text{dyn}} = 0.013$  yielding a total zig-zag distortion of  $z_{\text{tot}} = 0.902$ , which is noticeably smaller than  $z_{\text{min}} = 1.001$  for  $N_{\text{ph}} = 0$ . Well above the transition point the dynamically induced distortions are very small, for instance for  $V = 3.0$  and  $N_{\text{ph}} = 3$  calculations gave  $z_{\text{dyn}} = 0.0005$ , and  $z_{\text{stat}} = 1.290$  is only slightly smaller than  $z_{\text{min}} = 1.294$ .

From this analysis we conclude that using just static distortions gives qualitatively correct results but overestimates the lattice distortions, in particular, in the vicinity of the phase transition. The value of the order parameter in the full dynamical model with  $N_{\text{ph}} = \infty$  will therefore be somewhat smaller than in Sec. III A, as discussed above.

## VI. CONCLUSIONS

In this paper we investigated the influence of lattice effects on the charge ordering transition, the spectrum of kink excitations and dynamical susceptibilities of quarter-filled ladder systems and considered the  $\alpha'$ - $\text{NaV}_2\text{O}_5$  compound as an example. For this purpose we modified the Hamiltonian of the extended Hubbard model by terms which take into account the coupling of electrons to lattice distortions. The lattice rigidity  $\kappa$  and the Holstein coupling constant  $C$  used in our model were determined by first-principles band-structure calculations. The physical properties were calculated by the exact diagonalization technique. The results for the ground-state energy and the order parameter show

that by including static distortions, the phase transition is shifted significantly downward to lower values of the nearest-neighbor Coulomb interaction  $V$ . The calculated displacements of the vanadium ions due to the electron-lattice coupling in the charge ordered phase are in good agreement with experimental measurements.<sup>7</sup> We also found a virial theorem to be fulfilled to high precision for the terms in the Hamiltonian that couple to the lattice.

As low-energy excitations of the distorted ground state we considered kink excitations, where the charge order pattern changes along the ladder between two degenerate configurations. These kinks are long when  $m_{\text{CO}}^2$  is small, and become shorter with increasing order. The kink lengths and energies at small  $m_{\text{CO}}^2$  are comparable with those of a classical  $\phi^4$  model.<sup>12</sup>

Moreover, we studied the extended Hubbard-Holstein model to investigate the effect of dynamical phonons. Results showed that they have a strong influence on the charge order parameter in the vicinity of the phase transition. An analysis of the correlations of the dynamically induced distortions revealed that phonons indeed favor zig-zag lattice distortions. We showed that using just static distortions somewhat overestimates the actual value of the lattice distortion, but well away from the

transition point this dynamical effect is very small and a description by static distortions gives already accurate results.

In addition to these static properties we also calculated the dynamic charge and spin susceptibilities. We showed that the main features of these quantities are determined by the value of the order parameter and not by the way this value is achieved. From the spin susceptibility we extracted the effective magnetic exchange interaction along the ladder, which exhibits a pronounced decrease with increasing charge order. The magnitude of this parameter taken at  $V = 1.3, C = 0.35$  is in good agreement with the experimental inelastic neutron scattering data.<sup>31</sup>

### Acknowledgments

This work has been supported by the Austrian Science Fund (FWF), project No. P15520. M.A. and M.H. have been supported by the doctoral scholarship program of the Austrian Academy of Sciences. One of us (E.Y.S) is grateful to P. Lemmens and M.N. Popova for interesting discussions.

- 
- <sup>1</sup> E. J. W. Verwey, Nature (London) 144, 327 (1939), E. J. W. Verwey and P. W. Haayman, Physica (Amsterdam) 8, 979 (1941).
- <sup>2</sup> H. Smolinski, C. Gros, W. Weber, U. Peuchert, G. Roth, M. Weiden, and C. Geibel, Phys. Rev. Lett. **80**, 5164 (1998).
- <sup>3</sup> T. Ohama, H. Yasuoka, M. Isobe, and Y. Ueda, Phys. Rev. B **59**, 3299 (1999).
- <sup>4</sup> M. Isobe and Y. Ueda, J. Phys. Soc. Jpn. **65**, 1178 (1996).
- <sup>5</sup> M. N. Popova, A. B. Sushkov, S. A. Klimin, E. P. Chukalina, B. Z. Malkin, M. Isobe, and Y. Ueda Phys. Rev. B **65**, 144303 (2002).
- <sup>6</sup> E. Ya. Sherman, M. Fischer, P. Lemmens, P. H. M. van Loosdrecht, and G. Güntherodt, Europhys. Lett. **48**, 648 (1999).
- <sup>7</sup> J. Lüdecke, A. Jobst, S. van Smaalen, E. Morre, C. Geibel, and H. -G. Krane, Phys. Rev. Lett. **82**, 3633 (1999).
- <sup>8</sup> M.N. Popova, A.B. Sushkov, A.N. Vasil'ev, M. Isobe, and Y. Ueda, Pis'ma Zh. Eksp. Teor. Fiz. **65**, 711 (1997) [JETP Lett. **65**, 743 (1997)]
- <sup>9</sup> M. Fischer, P. Lemmens, G. Els, G. Güntherodt, E. Ya. Sherman, E. Morre, C. Geibel, and F. Steglich, Phys. Rev. B **60**, 7284 (1999).
- <sup>10</sup> J. Riera and A. Poilblanc, Phys. Rev. B **59**, 2667, (1999).
- <sup>11</sup> R. T. Clay and S. Mazumdar, cond-mat/0305479.
- <sup>12</sup> E. Ya. Sherman, C. Ambrosch-Draxl, P. Lemmens, G. Güntherodt, and P. H. M. van Loosdrecht, Phys. Rev. B **63**, 224305 (2001)
- <sup>13</sup> H. Seo and H. Fukuyama, J. Phys. Soc. Jpn. **67**, 2602 (1998).
- <sup>14</sup> P. Thalmeier and P. Fulde, Europhys. Lett. **44**, 242 (1998).
- <sup>15</sup> M. Mostovoy and D. I. Khomskii, Solid State Commun. **113**, 159 (2000), M. V. Mostovoy, D. I. Khomskii, and J. Knoester, Phys. Rev. B **65**, 064412 (2002)
- <sup>16</sup> M. Vojta, A. Hübsch, and R. M. Noack, Phys. Rev. B **63**, 045105 (2001); M. Vojta, R. E. Hetzel, and R. M. Noack, *ibid.* **60**, R8417 (1999).
- <sup>17</sup> E. Orignac and R. Citro, Eur. Phys. J. B **33**, 419 (2003).
- <sup>18</sup> M. Aichhorn, P. Horsch, W. von der Linden, and M. Cuoco, Phys. Rev. B **65**, 201101(R) (2002).
- <sup>19</sup> A. Hübsch, C. Waidacher, K. W. Becker, and W. von der Linden, Phys. Rev. B **64**, 075107 (2001).
- <sup>20</sup> M. Cuoco, P. Horsch, and F. Mack, Phys. Rev. B **60**, R8438 (1999).
- <sup>21</sup> Z. S. Popovic and F.R. Vukajlovic, Phys. Rev. B **59**, 5333 (1999); H. Wu and Q. Zheng, *ibid.* **59**, 15027 (1999); A. N. Yaresko, V. N. Antonov, H. Eschrig, P. Thalmeier, and P. Fulde, *ibid.* **62**, 15538 (2000); V. V. Mazurenko, A. I. Lichtenstein, M. I. Katsnelson, I. Dasgupta, T. Saha-Dasgupta, and V. I. Anisimov, *ibid.* **66**, 081104(R) (2002).
- <sup>22</sup> J. Spitaler, E. Ya. Sherman, C. Ambrosch-Draxl, and H. G. Evertz, Physica Scripta (to be published); J. Spitaler, E. Ya. Sherman, C. Ambrosch-Draxl, and H. G. Evertz, cond-mat/0404076.
- <sup>23</sup> E. I. Rashba, in *Excitons*, edited by E. I. Rashba and M. D. Sturge, (North-Holland, Amsterdam, 1982), p. 543.
- <sup>24</sup> K. Okunishi and N. Maeshima, Phys. Rev. B **64**, 212406 (2001).
- <sup>25</sup> J. des Cloizeaux and J. J. Pearson, Phys. Rev. **128**, 2131 (1962).
- <sup>26</sup> P. Horsch and F. Mack, Eur. Phys. J. B **5**, 367 (1998).
- <sup>27</sup> M. Weiden, R. Hauptmann, C. Geibel, F. Steglich, M. Fischer, P. Lemmens, and G. Güntherodt, Z. Phys. B **103**, 1 (1997).

- <sup>28</sup> C. Gros and R. Valentí, Phys. Rev. Lett. **82**, 976 (1999).
- <sup>29</sup> A. Hübsch, M. Vojta, and K. W. Becker, J. Phys.: Condens. Matter **11**, 8523 (1999).
- <sup>30</sup> A. Damascelli, D. van der Marel, M. Grüninger, C. Presura, T.T.M. Palstra, J. Jegoudez, and A. Revcolevschi, Phys. Rev. Lett. **81**, 918 (1998), A. Damascelli, C. Presura, D. van der Marel, J. Jegoudez, and A. Revcolevschi, Phys. Rev. **B 61**, 2535 (2000)
- <sup>31</sup> B. Grenier, O. Cepas, L. P. Regnault, J. E. Lorenzo, T. Ziman, J. P. Boucher, A. Hiess, T. Chatterji, J. Jegoudez, and A. Revcolevschi, Phys. Rev. Lett. **86**, 5966 (2001).
- <sup>32</sup> D. M. Edwards, Adv. Phys. **51**, 1259 (2002).
- <sup>33</sup> F. Marsiglio, Phys. Lett. A **180**, 280 (1993).
- <sup>34</sup> G. Wellein, H. Röder, and H. Fehske, Phys. Rev. B **53**, 9666 (1996).
- <sup>35</sup> F. Marsiglio, Physica C **244**, 21 (1995).